Developing high intensity ultrasonic cleaning (HIUC) for post-processing additively manufactured metal components

Author names and affiliation

W.X. Tan[a], K.W. Tan[a*], K.L. Tan[b*] ,

a) School of Materials Science and Engineering, Nanyang Technological University, Singapore 639798, Singapore.
b) Advanced Remanufacturing and Technology Centre, 3 Cleantech Loop, #01/01 CleanTech Two, Singapore 637143, Singapore.

*Corresponding authors.

K.L. Tan: Tel.: (+65) 9008 5430, Email address: tan_kai_liang@artc.a-star.edu.sg

K.W. Tan: Tel.: (+65) 67906231, Email address: kwtan@ntu.edu.sg

Abstract

The high energy phenomenon of cavitation bubble collapses has enabled numerous applications, including cleaning. In ultrasonic cleaning, cavitation intensity is typically lower than in other applications, such as sonochemistry and material processing. However, there has been an emerging application in intense cleaning of metal additively manufactured (AM) components. The presence of partially melted powders on AM surfaces is undesirable, contributing to high surface roughness and posing contamination risks during usage. We designed a high-intensity cavitation cleaning process that has significantly higher inertial cavitation intensity – i.e., erosion potential – than a conventional ultrasonic cleaning tank. Through acoustic signal characterisation, we showed that placing transducer sets on four sides of the tank could effectively focus and generate high-amplitude pressure waves directed towards the central region. Strong subharmonic signals indicate intensely inertial cavitation throughout the tank. Cavitation intensities were measured at various locations to understand the wave transmission characteristics and distribution patterns. Our results show that the cavitation intensity distribution is highly dependent on the height position. Finally, we demonstrated that the high intensity ultrasonic cleaning (HIUC) process could remove partially melted powders from an AM surface – which was not possible through conventional ultrasonic cleaning. HIUC could lead to higher cleaning efficiency and enhanced AM specimen cleanliness.

Keywords

Ultrasonic cavitation, focused ultrasonic wave, cavitation characterisation, acoustic signal analysis, ultrasonic cleaning

1. Introduction

The collapse of high-intensity ultrasonic cavitation bubbles, and their associated phenomena, find wide industrial applications including cleaning [1], sonochemistry [2], material processing [3] and wastewater treatment [4]. Ultrasonic excitation in these applications can be broadly categorised into two configurations: (i) ultrasonic bath and (ii) ultrasonic horn (or sonotrode). An ultrasonic bath involves multiple piezoelectric transducers transmitting low-amplitude vibrations to the target liquid. In an ultrasonic horn setup, a step-up booster horn is used to amplify the transducer's vibrational amplitude, thereby significantly increasing the cavitation intensity [5].

A conventional ultrasonic bath, such as an ultrasonic cleaner, typically induces cavitation above the inertial threshold. Bubbles nucleate, grow and finally collapse according to the acoustic cycle. When bubbles collapse, microjet formation generate concentrated shearing and lifting force on the dirt particles, leading to dislodgement [6]. Despite the cleaning capabilities, bubbles typically do not grow to more than few micrometres, thereby restricting its collapse strength. On top of individual bubble dynamics, bubble streaming flow also contributes greatly to the cleaning action and contaminant removal [7]. Comparatively, ultrasonic horns could generate highly inertial cavitation, with bubbles growing to maximum sizes of few hundreds of micrometres. The bubble collapse phenomena generate intense shockwave and microjets [8] that are capable of eroding metal surfaces [9] and cleaning polymer-based 3D printed projects [10]. A recent study by Priyadarshi et al. [11] suggested that the collapse and rebound of oscillating bubble clusters also contributed to de-agglomeration of oxides. However, this intense cavitation effects are limited to the small conical shape cavitation zone attached to the horn surface [12, 13]. This is due to the poor transmissibility of ultrasonic waves through the bubbly liquid – a discontinuous medium [14]. This poses a huge challenge to the scalability of an ultrasonic horn setup in cleaning large and complex components.

There has been an emerging cleaning application in post-processing metal additively manufactured (AM) components. A major downside of as-built metal AM components is the inherently poor surface roughness – of which the presence of partially melted powder is a main contributor [15]. During the layer-by-layer building process, heat dissipation from the laser source partially melts the surrounding powders at the contour edges, resulting in the partial attachments of powders [16]. The extent of powder attachment varies according to the build orientation. At the top (0°) and upskin surfaces (0°-90°), the melt pool is relatively contained, and partial melting of adjacent powders is largely avoided. The presence of partially melted powders is especially significant on side (90°) and downskin surfaces (90°-180°).

Electrochemical and chemical processes have been widely deployed to remove partially melted powders and reduce the average surface roughness, *Ra*, on complex AM components. Chang et al. [17] demonstrated an overpotential electrochemical polishing at an elevated temperature of 50 – 60°C to remove sticking particles. Lyczkowska et al. [18] used a combination of ultrasonic bath and chemical polishing to clean lattices. An ultrasonic bath was effective in removing loose, unmelted AM powders, while chemical polishing further etched away the partially melted powders. However, chemical-based processes tend to result in a large amount

of material removal, leading to dimension losses of more than 20% [19]. This effect would be especially significant components with thin structures, such as lattices [20]. To minimise dimensional losses, Tan and Yeo [21] deployed an ultrasonic horn setup to clean and finish an AM as-built side surface (90°). They demonstrated that targeted powder removal by cavitation bubble collapses alone could lead to *Ra* improvement of more than 30%. However, the ultrasonic horn setup is limited by the small cavitation zone near the ultrasonic horn [22]. An ultrasonic device with a larger, highly intense cavitation zone is desired for an actual complex AM component.

Researchers have proposed cavitation vessels with unique designs to enhance cavitation intensity in large area processing for sonochemical and cleaning applications [23, 24]. Hodnett et al. [25] designed a cylindrical vessel with rows of 25 kHz piezoelectric transducers mounted onto the side wall, radiating ultrasonic waves into the central volume. They measured more than double peak-negative acoustic pressure at the central region as compared to other regions within the tank [26]. This geometrical focusing effect has also been explored with high-intensity 20 kHz ultrasonic horns [27]. Pishchalnikov et al. [28] outlined a spherical resonator design, and demonstrated that the focused wave at the central region could overcome extreme static pressure. In addition to the tank design, transducer locations are also critical in determining cavitation distribution and intensity. Asakura et al. [29] reported higher sonochemical efficiency when transducers are located at side walls, compared to the bottom wall. More recently, Tangsopa et al. [30] optimised transducer placement in an industrial cleaning tank through harmonic response analysis to achieve high cleaning efficacy. They suggested that placing transducers both at side and bottom walls result in a more uniform cleaning within the ultrasonic tank. While these studies focused mostly on the cleaning efficacy and uniformity, they are still useful inspirations in the design of a highly intense process for de-powdering AM components.

In the present work, we designed an ultrasonic cleaning machine with geometrical focusing of ultrasonic waves. Immersible transducer sets were placed on the sides of an ultrasonic tank to generate a highly intense central cavitation zone – with sufficient intensity to remove partially melted powders from AM surfaces. The process is termed as high-intensity ultrasonic cleaning (HIUC). We evaluated the cavitation intensity distribution within the tank experimentally via a pressure hydrophone. We then demonstrated the HIUC process could de-powder AM cobalt chrome specimens significantly, which is not possible in conventional ultrasonic cleaning setups.

2. Methods

2.1 High-intensity ultrasonic cavitation machine

Figure 1 shows the design overview of our HIUC machine. The main tank has a cylindrical inner profile (diameter: 440 mm, height: 420 mm) to enhance the cavitation intensities through acoustic wave interference. The volume capacity is approximately 60 L. A total of four rectangular immersible transducer sets (28 kHz) were located within the cylindrical tank on all four sides, as shown in Figure 2. The dimensions of each transducer set are 170 mm × 75 mm

× 310 mm (L × W × H). Within the transducer set, there are six individual piezoelectric transducer elements, each with a maximum power output of 100 W. Immersible transducers transmit energy directly into the working fluid, thus eliminating possible energy losses due to poor bonding in conventional transducers. The maximum power output of the HIUC machine is 2.4 kW, powered by two ultrasonic generators – each connecting to two transducer sets. The distance between the opposing transducer sets is 260 mm, a multiple of the acoustic wavelength (λ) in water (approximately 52 mm at 28 kHz) [31]. This allows the acoustic wave to interfere constructively, generating an intense central cavitation zone.

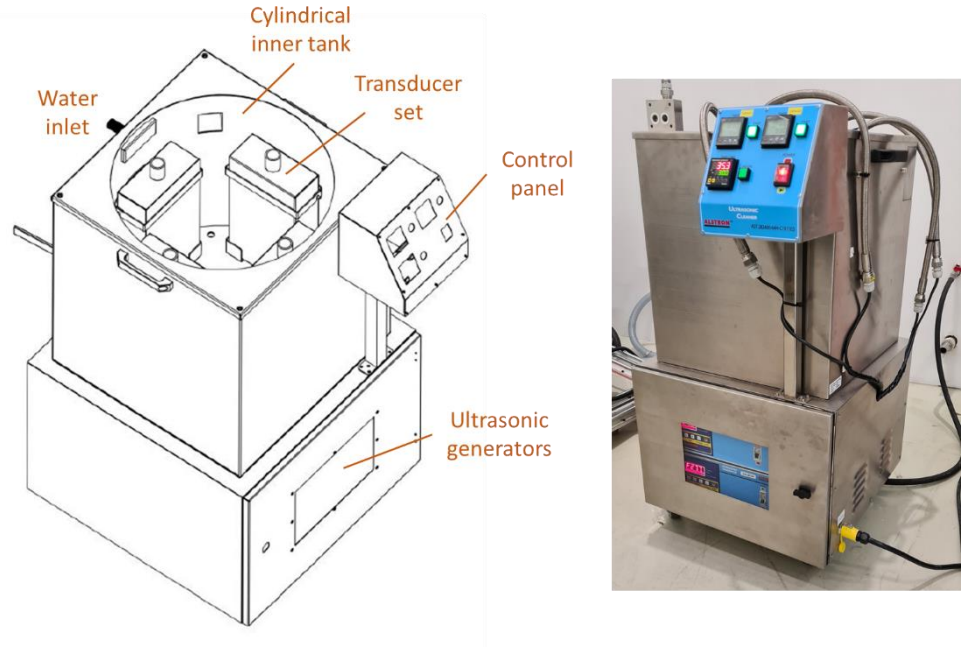

Figure 1: Overview of HIUC machine design

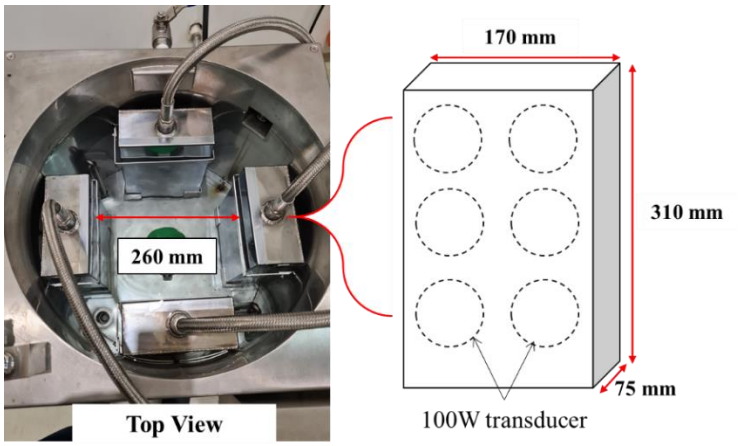

Figure 2: Illustration of transducer arrangement within the tank

2.2 Acoustic characterisation

A pressure hydrophone (Type 8103, Brüel & Kjær) was used to obtain the acoustic emissions within the cavitation vessel. The hydrophone has a flat frequency response from 0.1 Hz to 180 kHz with a receiving sensitivity of −211.2 dB re 1 V/µPa. A holding jig was designed to clamp

and hold the hydrophone within the cavitation vessel (Figure 3). The holding jig is mounted onto a X-Y stage, controlled by a linear axis controller with precision up to 0.001 mm.

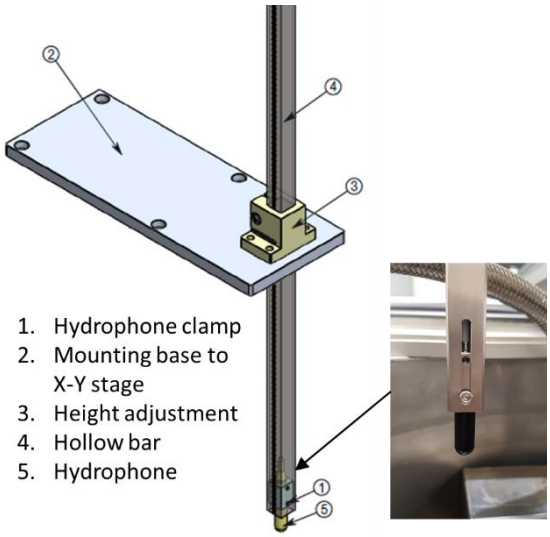

Figure 3: Hydrophone holding jig

In each measurement, acoustic signals were recorded over 10 s duration, corresponding to approximately 280 000 acoustic cycles. A total of 3 measurements were obtained for each specimen to ensure the repeatability of the signals. A Fast Fourier Transform (FFT) was then performed to obtain pressure signals across the frequency domain. A Hanning window was applied, and the frequency resolution was fixed at 5 Hz for all analysis. Cavitation intensity was estimated through both fundamental (f_0) and subharmonic frequency ($f_0/2$) [13, 32]. To validate the acoustic emission results, aluminium foil erosion test was also conducted. Heavy duty aluminium foil (24 µm thickness) was cut into strips with dimensions of 15 mm × 75 mm (H × L) and attached to the holding jig. Erosion was analysed with an image processing software (ImageJ) to estimate the erosion area.

2.3 Experimental conditions

Tap water (Singapore Public Utilities Board) was used as the working fluid, with 5 min degassing at 100% power before each run. Figure 4 shows the measurement position coordinate system (x, y, z) within the ultrasonic tank. A preliminary study on the effect of temperature (T) and ultrasonic power (P) was first conducted at the central location of the tank (123, 123, 155). Table 1 lists the detailed experimental conditions. Following which, intensity variation with the height level (z) was studied at the central location of the tank (123, 123, z), at intervals of 10 mm. Finally, a X-Y cavitation intensity contour mapping was conducted at two different height levels – z = 100 mm and 155 mm from the bottom tank, respectively. The intervals between each measurement point were kept at 20 mm along both X and Y direction (the hydrophone diameter is 9.5 mm). In both height variation and X-Y contour map study, P was set at 80% and T was 30 °C.

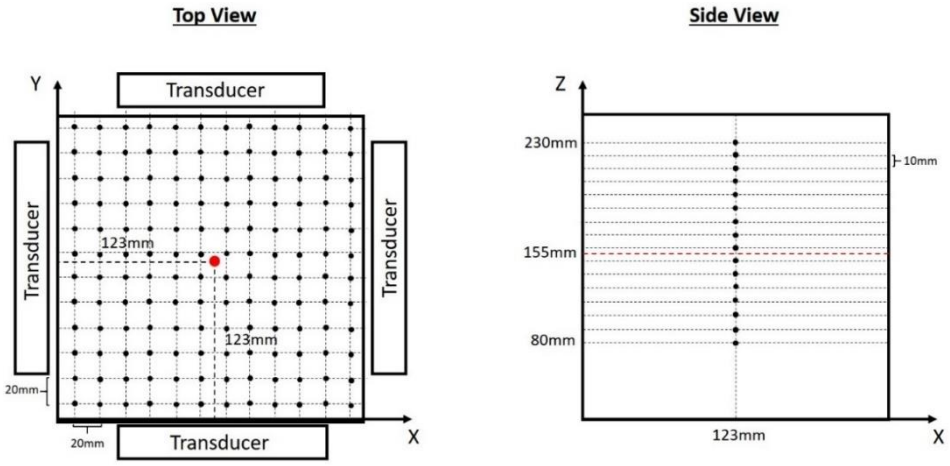

Figure 4: Measurement positions of acoustic emissions

Table 1: Experimental conditions

Parameters	Conditions
Ultrasonic power (%)	20, 30, 40, 50, 60, 80, 100
Temperature (°C)	30, 40, 50, 60

2.4 AM specimen and cleaning characterisation

The AM specimen used in this study was cobalt chrome manufactured by direct laser metal sintering (EOS M290, EOS GmbH). The material properties are detailed in the manufacturer's material data sheet (EOS Cobalt Chrome MP1). The default building parameters were used. The specimen has an overall dimension of 50 mm × 30 mm × 12 mm (H × L × W) with lattice designs (Figure 5(a)). After the AM building process, specimens were wire-cut from the building plate without other post-processing. Scanning electron microscope (EVO SEM, Zeiss) was used to observe the surface morphology at the lattice nodes and struts (Figure 5(b)). Specimen mass was measured using an analytical precision weighing balance with a resolution of 0.1 mg.

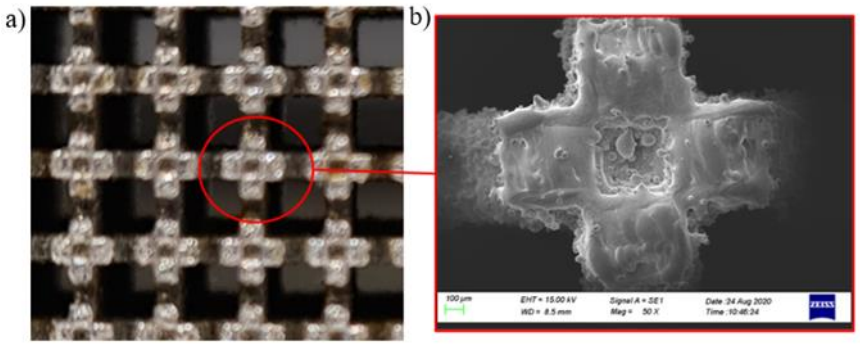

Figure 5: (a) AM lattice; (b) observation of a single lattice node under SEM

3 Results and Discussion

3.1 Acoustic emissions in HIUC machine

Figure 6 shows the typical acoustic emissions measured at the central location (123, 123, 155) of the HIUC machine at 30 °C and 100% power input (2400 W). The power density was approximately 38 W/L. A sharp fundamental peak corresponding to the ultrasonic frequency is present at 28 kHz. A distinct subharmonic signal at 14 kHz ($f_0/2$) and numerous ultraharmonics ($3f_0/2$, $2f_0$) were also observed on the acoustic spectra. These indicate the presence of strong inertial cavitation around the vicinity of the hydrophone. The measurements were compared against the acoustic signals obtained from a conventional ultrasonic cleaner (HCS8200GT, HCS Scientific & Chemical) with a lower power density (31W/L) at 35 kHz. The selected cleaner was typically deployed to remove loose powders from AM components. In the conventional cleaner, no distinct subharmonic peak was observed. In addition, the cavitation noise floor is approximately 20 dB lower than the HIUC machine. These suggest that with a 20% higher input power density, our HIUC machine is capable of significantly higher cavitation intensity than the conventional cleaner. In subsequent analysis, the subharmonic signal intensity would be used as an indicator of inertial cavitation intensity.

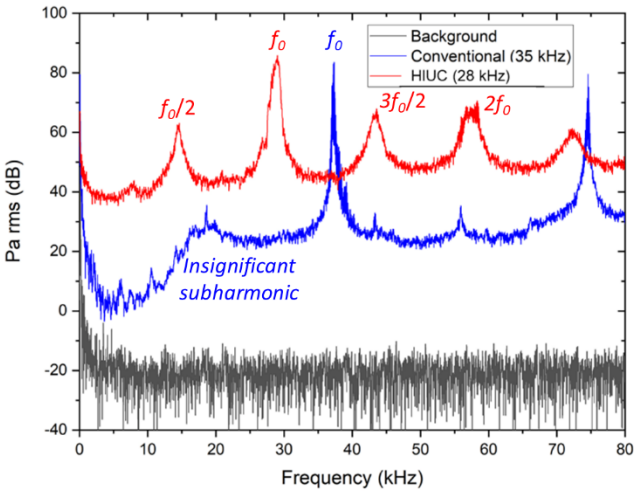

Figure 6: Comparison of acoustic emissions between HIUC and a conventional ultrasonic cleaner

Figure 7 shows the inertial cavitation intensity contour maps at two configurations. With only one pair of transducer sets, inertial cavitation was detected but closer to the transducer surfaces. The cavitation intensity measured in the central region was lower than the other regions. However, when all four transducer sets were switched on, a high-intensity central region was formed due to the geometrical focusing effect. The combined inertial cavitation intensity was also more evenly spread around the ultrasonic tank.

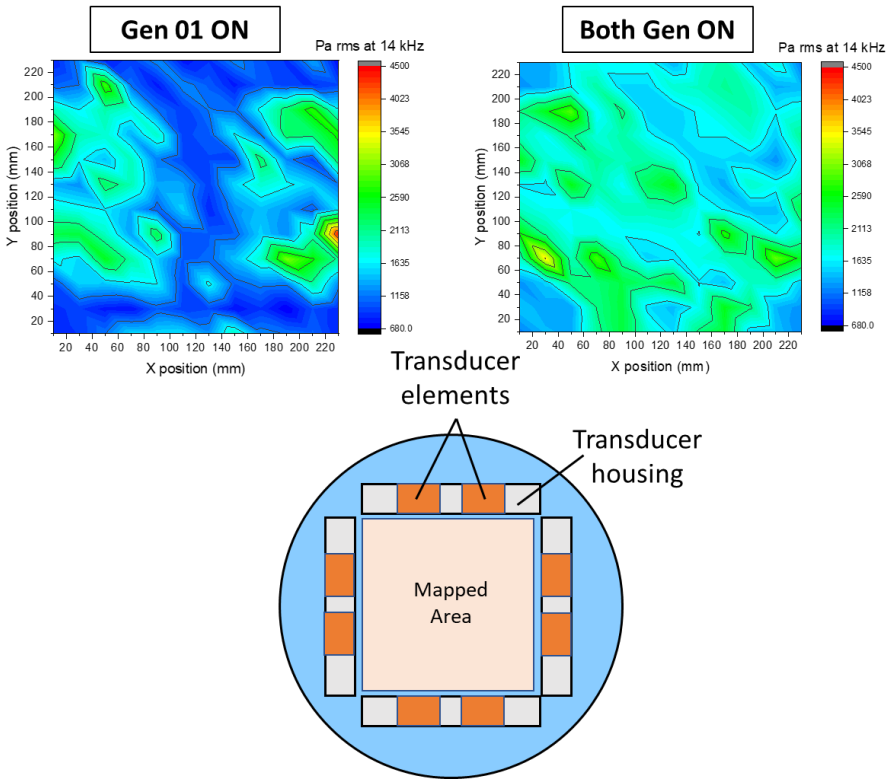

Figure 7: Intensity contour map demonstrating the geometrical focusing effect when all four transducer sets are switched on (*z* = 155 mm, *P* = 100%, *T* = 30 °C).

3.2 Effect of power and temperature

Figure 8 shows the variation of subharmonic signal intensity at the respective ultrasonic power and fluid temperature levels. At lower *T* values (30 and 40 °C), inertial cavitation is negligible at low *P*, evident by the absence of subharmonic signals. Subharmonic peaks appear only at *P* ≥ 40%. Signal intensity increases with ultrasonic power, then dips slightly at the maximum power of 100%. The slight dip could be attributed to the wave attenuation at excessive acoustic power levels. At higher *T* levels (50 and 60 °C), the trends were reversed. Significant subharmonic peaks were observed even at the lowest *P* of 20%. This could be attributed to the higher vapour pressure as the fluid temperature increases. At 60 °C, the vapour pressure of water is at 19.90 kPa, as compared to 4.24 kPa at 30 °C. The higher vapour pressure means that a lower amplitude pressure wave is required to induce bubble nucleation [33]. However, the ensuing cavitation bubble collapses were less intense due to the high vapour pressure contributing to the cushioning effect. This slows down the bubble wall collapse velocity and reduces the shockwave intensity [34]. Therefore, the cavitation intensity did not increase with the increase in input power.

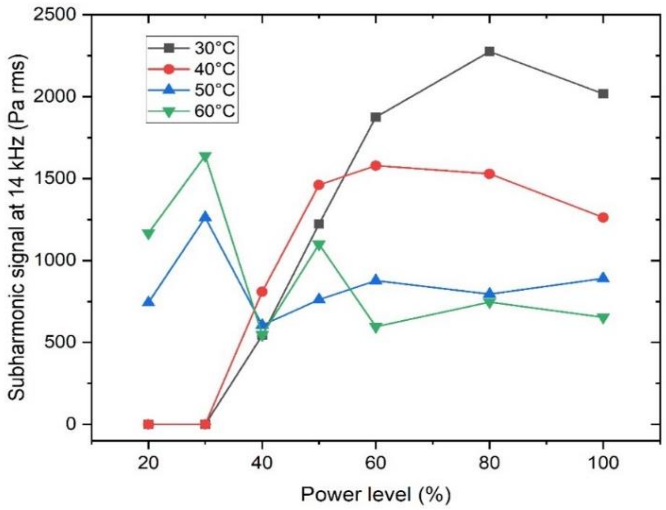

Figure 8: Effect of temperature and input power on the subharmonic signal intensity

3.3 Cavitation intensity distribution

3.3.1 Inertial cavitation intensity variation with *z*

Intensity mapping could shed light on the cavitation characteristics of the developed HIUC machine. Figure 9 shows the subharmonic signal intensity across the height levels, measured at the central X-Y location (123, 123, *z*). Two clear peaks were observed, indicating significant inertial cavitation at *z* = 110 mm and 200 mm, respectively. The intensities at these two height levels are at least 5 times higher than the intensity recorded at the height of 140 mm and 230 mm. Referring to the transducer element positions within the ultrasonic tank (Figure 9), the lowest inertial cavitation intensities correspond to the level of individual transducer elements. On the contrary, the peak intensities occur at the height levels between the rows of transducer elements.

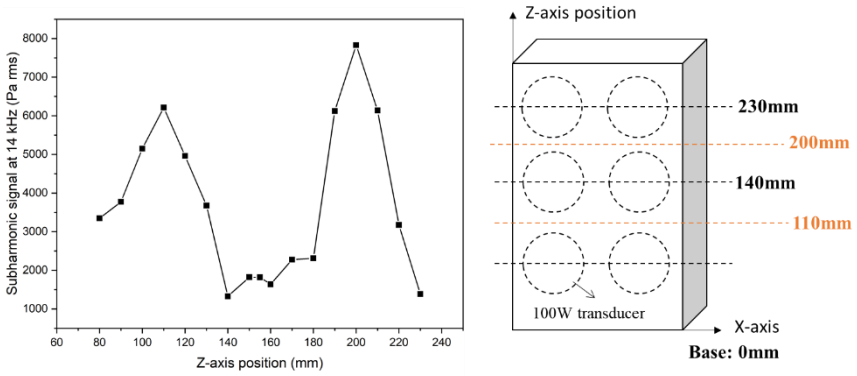

Figure 9: Subharmonic signals at various *z* levels (*P* = 80%, *T* = 30 °C)

We propose that the shielding effect of bubble clusters near the transducers contribute to the observed divergence in intensities between the height levels [35]. Figure 10 illustrates the wave transmission mechanism within the ultrasonic tank. At *z* = 140 and 230 mm, bubble clusters form near to the transducers, thereby acting as a discontinuous medium, thereby affecting the speed of sound and wave pattern. Waves travelling in a straight line to the central region face

energy losses and ineffective transmission. At z = 200 mm, the lack of bubble clusters in the vicinity allows waves to travel further to the central region. Constructive wave interference from all four transducer sets forms the strong cavitation intensity at the central region.

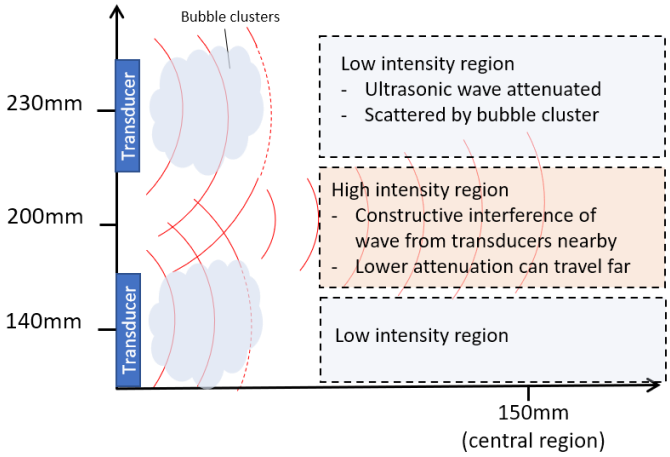

Figure 10: Illustration of shielding effect

3.3.2 X-Y cavitation intensity contour maps

Full cavitation intensity mapping was then conducted at two height levels: z = 155 mm and 200 mm. The height levels were selected to further understand the wave transmission and cavitation intensity distribution characteristics as discussed above. Figure 11 shows the acoustic signal intensity distribution at both f_0 and $f_0/2$. At z = 155 mm (Figure 11(a)), intense f_0 signals were concentrated at the regions surrounding the transducer elements. This corresponded to the ultrasonic pressure waves directly transmitted from the transducer elements. The high amplitude pressure waves led to increased bubble population and inertial cavitation activity. The resulting bubbly liquid around the transducers attenuated the pressure waves significantly, leading to the low f_0 signals measured at the central region (less than half than at around the transducer elements). A recent study by Khavari et al. [36] showed photographic evidence of wave attenuation when vapour clouds are present in the vicinity of an ultrasonic transmitter. With poor propagation of the fundamental acoustic waves, the central region did not have significant inertial cavitation activity as compared to other regions of the ultrasonic tank.

At z = 200 mm, the cavitation intensity distribution was distinct from z = 155 mm. The ultrasonic waves at fundamental frequency were more evenly spread around the transducer housing area. Without the direct transmission of pressure waves from the elements, there was no significant bubble activity near the transducer housing. This led to further wave propagation from the transducer element to the central region, which resulted in constructive wave interferences and significant peak f_0 signals measured at the central region. Consequently, the subharmonic signals also peaked, with pockets of high inertial cavitation activity in the central region. These findings further validate the hypothesis presented in Figure 10. At levels where transducer elements are located (i.e., z = 140, 230 mm), inertial cavitation regions are concentrated near the transducer. At levels between the rows of transducer elements (i.e., z = 110, 200 mm), wave attenuation is less pronounced, leading to constructive wave interference,

peak negative pressure and enhanced inertial cavitation activity at the central region. The geometrical focusing effect is dependent on the height level within the HIUC machine.

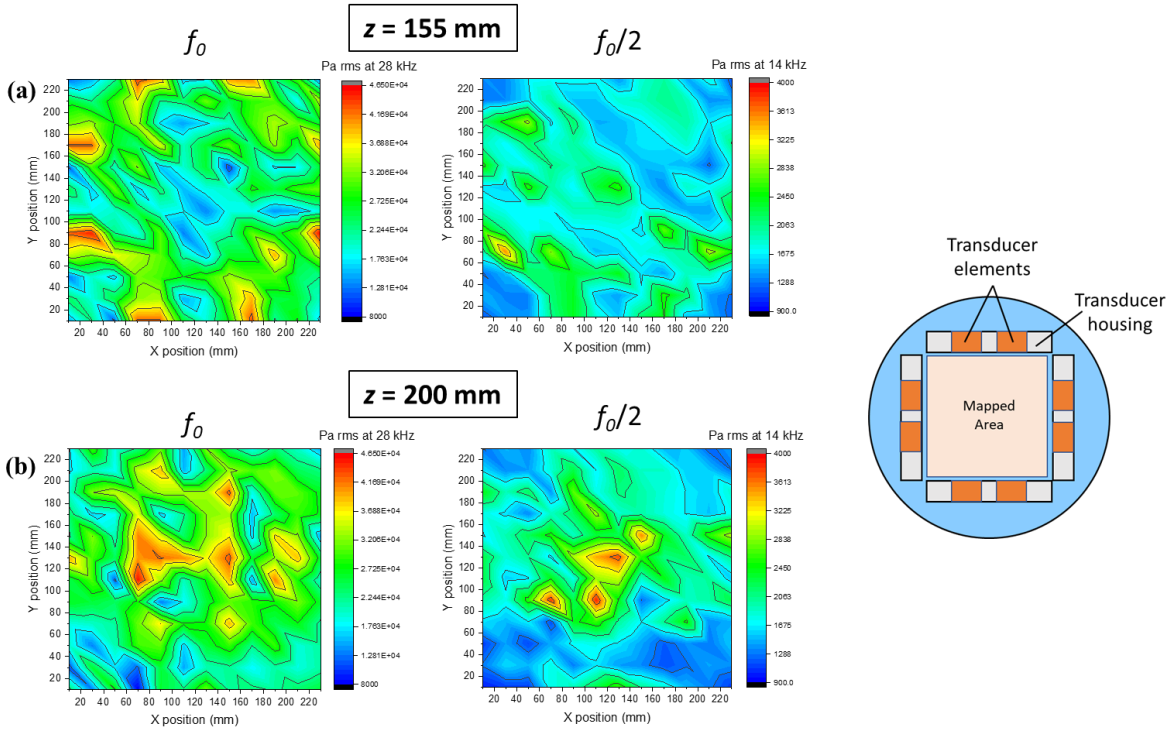

Figure 11: Intensity contour mapping of fundamental (f_0) and subharmonic ($f_0/2$) acoustic signals at (a) z = 155 mm and (b) z = 200 mm.

Aluminium foil erosion test was conducted to verify our interpretation from the acoustic signal emission measurements. Aluminium foil (heavy duty, 24 µm thickness) was cut into rectangular strips, then wrapped around the hollow bar in the hydrophone fixture (Figure 3) and immersed into the test locations. Two samples were conducted at each test location. Figure 12(a) shows that at the central region, the foil erosion at z = 200 mm is more pronounced than at z = 155 mm after 5 s exposure. This corresponds to the results in Figure 9 and Figure 11, validating the higher inertial cavitation activity at z = 200 mm. Figure 12(b) plots the average foil erosion area against the subharmonic signals obtained from the hydrophone. The positive correlation confirms that the subharmonic signal is a useful indicator of inertial cavitation intensity and erosion potential.

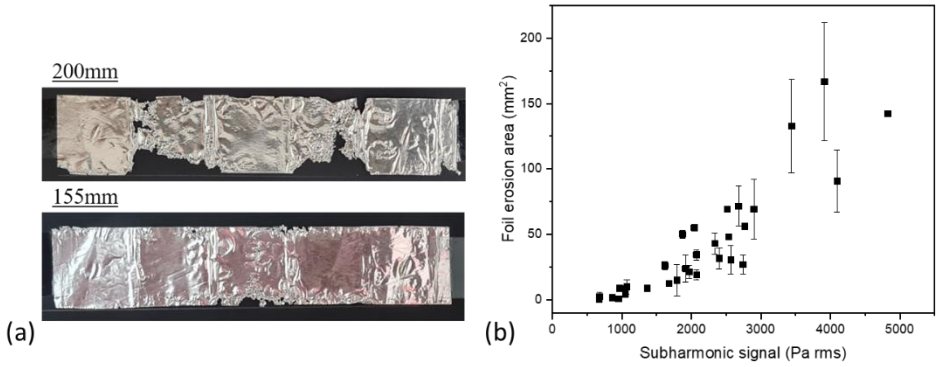

Figure 12: (a) Erosion pattern observed at the central region: z = 200 mm (above) and z = 155 mm (below); (b) Average foil erosion area against subharmonic signal. Error bar indicates deviation between runs.

3.4 Cleaning and de-powdering of metal AM surfaces

With detailed understanding of the cavitation intensity distribution in our HIUC machine, the AM specimen cleaning test was conducted at P = 80%, T = 30 °C and position of (123, 123, 200). Figure 13(a) highlights the mass loss comparison between AM specimens immersed in a conventional ultrasonic cleaner and the HIUC machine. The same workpiece-transducer orientation was used in both machines. In HIUC, mass loss was 200% higher than conventional ultrasonic cleaning after 2 hrs. After conventional cleaning, many partially melted powders remained on the surface (Figure 13(b)). These powders have relatively higher bond strength to the component substrate than loose powders. Without sufficient shearing energy from bubble collapses, further removals would not be possible, even with longer cleaning duration. To demonstrate HIUC's capability, the specimen after conventional cleaning was further processed in the HIUC machine. Most partially melted powders were removed through HIUC. This demonstrates that the HIUC machine has significantly higher cavitation intensity, and is capable of removing powders with higher degree of bonding to the surface.

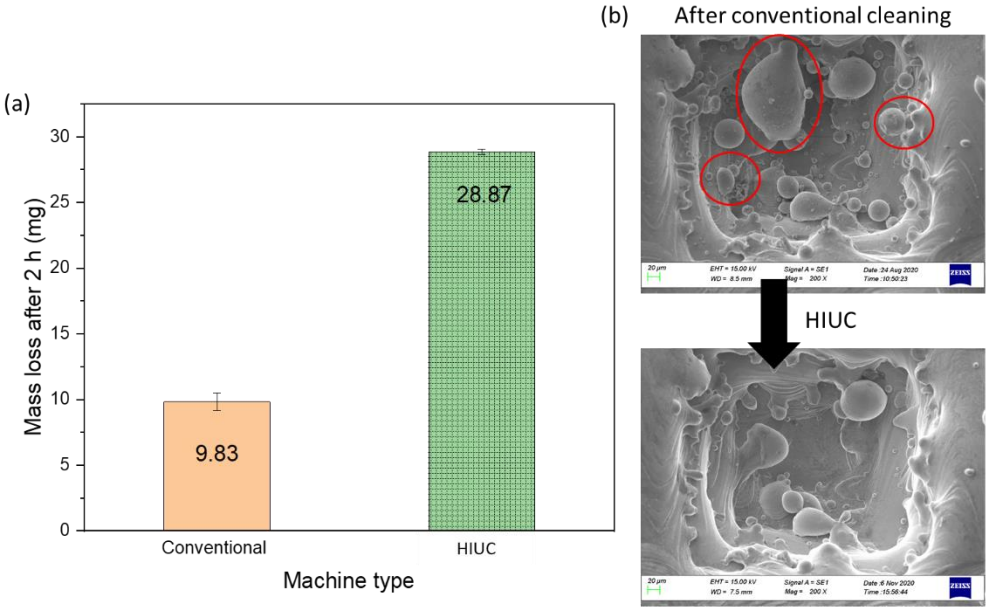

Figure 13: (a) Mass loss comparison between a conventional ultrasonic cleaner and HIUC; (b) SEM observation after conventional ultrasonic cleaning (top) and further HIUC (bottom)

Figure 14(a) shows the surface morphological as a function of HIUC processing time. Images were captured at the exact component location for observation. Surface irregularities were progressively removed up to the trial duration of 600 min. A close-up examination (Figure 14(b)) shows that powders were fractured at the bonding neck areas, resulting in a clean and complete removal from the surface. Repeated bubble collapses generate shearing energy and propagate cracks along the bonding neck, leading to failure and powder dislodgement. The adhesion strength between partially melted powders and the substrate are estimated to be around 20 – 100 MPa [37], based on single particle bonding strength of cold-sprayed powders. There was no surface damage or erosion pits visible on the remaining surface. Figure 15

describes the mass loss rate over processing time. The initial mass loss rate was the highest, with many loose powders that were easily removed. The mass loss rate slowed down over time reaching steady state, as the remaining powders had higher bonding strength to the surfaces.

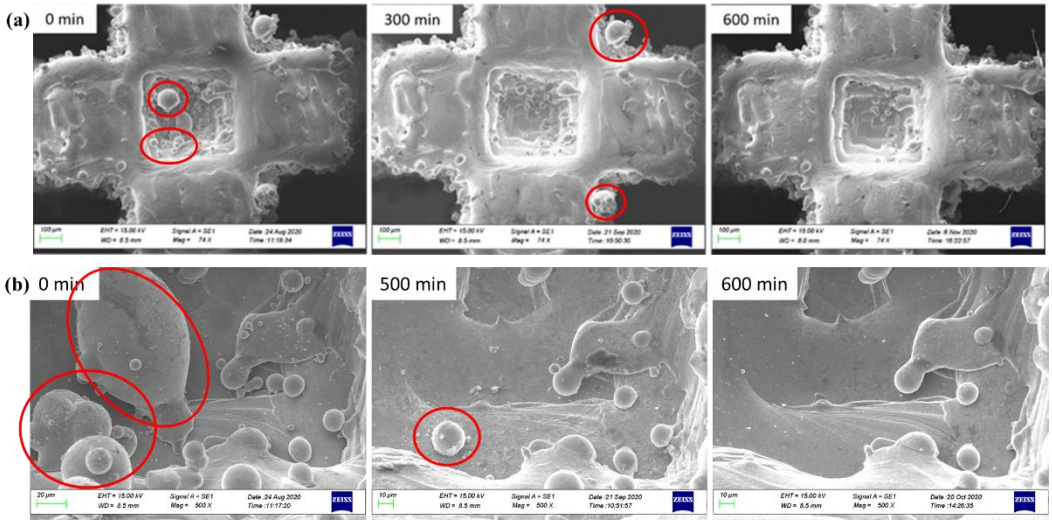

Figure 14: Surface morphological changes up to 600 min HIUC cleaning: (a) overview of structure at 74x, (b) close up examination at 500x

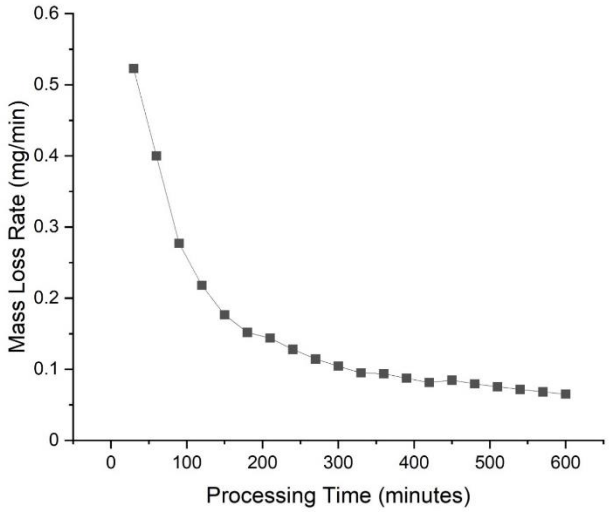

Figure 15: Mass loss rate over time

4. Conclusions

In this study, a new high-intensity cavitation cleaning machine was designed and fabricated to clean and de-powder AM components. As a contrary to conventional cleaners, immersible transducer sets were placed on the sides of the ultrasonic tank to generate geometrically focused waves towards the central region. The strong presence of subharmonic acoustic emission shows that the designed machine could generate inertial cavitation throughout the ultrasonic tank. Results show that there are regions of intense inertial cavitation activities with the highest erosion potential. The regions are dependent on the height levels and wave transmission characteristics. At levels directly corresponding to the transducer element, bubble clouds tend

to form near the transducer, restricting wave propagation. Between rows of transducer elements, ultrasonic wave could propagate further, leading to a central region with high-amplitude peak pressures and intense inertial cavitation.

Currently, conventional ultrasonic cleaning is used extensively in the AM industry for post-AM component cleaning. However, this process is only capable of removing loose, unmelted powders. To remove partially melted powders, or powders with higher bonding strength to the component substrate, intensely inertial cavitation would be required. We demonstrated that HIUC has the potential to remove partially melted powders and improve cleaning outcomes. Despite the enhanced cavitation intensity, no visible surface damage or erosion was observed after the HIUC process. Moving forward, the design of high-intensity ultrasonic cleaning could be further improved through process simulation and modelling. With enhanced powder removal capability, AM component surface roughness could also be improved significantly after HIUC. Explorations could also be expanded to other AM materials and specimen designs.

Acknowledgement

This work was conducted within the Advanced Remanufacturing and Technology Center, Singapore and supported under the core research funding of the Data-Driven Surface Enhancement Group. Deep appreciation also goes to Prof Yeo Swee Hock and Dr. Nagalingam Arun Prasanth for the lending of the hydrophone equipment.

CRediT Authorship Statement

Wei Xin Tan: Investigation, Methodology, Analysis, Writing – Original Draft **Kwan Wee Tan:** Writing – Review and Edit **Kai Liang Tan:** Conceptualisation, Investigation, Writing – Review and Edit, Visualization, Funding acquisition

References

[1] T. J. Mason, "Ultrasonic cleaning: An historical perspective," *Ultrasonics Sonochemistry*, 2016. **29**: 519–523.

[2] N. Pokhrel, P. K. Vabbina, and N. Pala, "Sonochemistry: Science and Engineering," *Ultrasonics Sonochemistry*, 2016. **29**: 104–128.

[3] D. G. Eskin *et al.*, "Fundamental studies of ultrasonic melt processing," *Ultrasonics Sonochemistry*, 2019. **52**: 455–467.

[4] J. Bandelin, T. Lippert, J. E. Drewes, and K. Koch, "Cavitation field analysis for an increased efficiency of ultrasonic sludge pre-treatment using a novel hydrophone system," *Ultrasonics Sonochemistry*, 2018. **42**(December 2017): 672–678.

[5] H. M. Santos, C. Lodeiro, and J.-L. Capelo-Martnez, "The Power of Ultrasound," in *Ultrasound in Chemistry: Analytical Applications*, Wiley-VCH, 2009, 1–16.

[6] G. L. Chahine, A. Kapahi, J.-K. Choi, and C.-T. Hsiao, "Modeling of surface cleaning by cavitation bubble dynamics and collapse," *Ultrasonics Sonochemistry*, 2016. **29**: 528–549.

[7] T. Yamashita and K. Ando, "Low-intensity ultrasound induced cavitation and streaming in oxygen- supersaturated water: Role of cavitation bubbles as physical cleaning agents," *Ultrasonics sonochemistry*, 2019. **52**(June 2018): 268–279.

[8] I. Tzanakis, D. G. Eskin, A. Georgoulas, and D. K. Fytanidis, “Incubation pit analysis and calculation of the hydrodynamic impact pressure from the implosion of an acoustic cavitation bubble,” *Ultrasonics Sonochemistry*, 2014. **21**(2): 866–878.
[9] J. R. Laguna-Camacho, R. Lewis, M. Vite-Torres, and J. V. Méndez-Méndez, “A study of cavitation erosion on engineering materials,” *Wear*, 2013. **301**(1–2): 467–476.
[10] B. Verhaagen, T. Zanderink, and D. Fernandez Rivas, “Ultrasonic cleaning of 3D printed objects and Cleaning Challenge Devices,” *Applied Acoustics*, 2016. **103**: 172–181.
[11] A. Priyadarshi *et al.*, “Mechanisms of ultrasonic de-agglomeration of oxides through in-situ high-speed observations and acoustic measurements,” *Ultrasonics Sonochemistry*, 2021. **79**: 105792.
[12] X. Ma, B. Huang, G. Wang, and M. Zhang, “Experimental investigation of conical bubble structure and acoustic flow structure in ultrasonic field,” *Ultrasonics Sonochemistry*, 2017. **34**: 164–172.
[13] K. L. Tan and S. H. Yeo, “Bubble dynamics and cavitation intensity in milli-scale channels under an ultrasonic horn,” *Ultrasonics Sonochemistry*, 2019. **58**: 104666.
[14] O. Louisnard, “A simple model of ultrasound propagation in a cavitating liquid. Part I: Theory, nonlinear attenuation and traveling wave generation,” *Ultrasonics Sonochemistry*, 2012. **19**(1): 56–65.
[15] T. Debroy *et al.*, “Additive manufacturing of metallic components – Process , structure and properties,” *Progress in Materials Science*, 2018. **92**: 112–224.
[16] G. Strano, L. Hao, R. M. Everson, and K. E. Evans, “Surface roughness analysis, modelling and prediction in selective laser melting,” *Journal of Materials Processing Technology*, 2013. **213**(4): 589–597.
[17] S. Chang *et al.*, “Highly effective smoothening of 3D-printed metal structures via overpotential electrochemical polishing,” *Materials Research Letters*, 2019. **7**(7): 282–289.
[18] E. Łyczkowska, P. Szymczyk, B. Dybała, and E. Chlebus, “Chemical polishing of scaffolds made of Ti–6Al–7Nb alloy by additive manufacturing,” *Archives of Civil and Mechanical Engineering*, 2014. **14**(4): 586–594.
[19] V. Urlea and V. Brailovski, “Electropolishing and electropolishing-related allowances for powder bed selectively laser-melted Ti-6Al-4V alloy components,” *Journal of Materials Processing Technology*, 2017. **242**: 1–11.
[20] G. Pyka, G. Kerckhofs, I. Papantoniou, M. Speirs, J. Schrooten, and M. Wevers, “Surface roughness and morphology customization of additive manufactured open porous Ti6Al4V structures,” *Materials*, 2013. **6**(10): 4737–4757.
[21] K. L. Tan and S. H. Yeo, “Surface modification of additive manufactured components by ultrasonic cavitation abrasive finishing,” *Wear*, 2017. **378**–**379**: 90–95.
[22] K. L. Tan and S. H. Yeo, “Surface finishing on IN625 additively manufactured surfaces by combined ultrasonic cavitation and abrasion,” *Additive Manufacturing*, 2020. **31**.
[23] S. Asgharzadehahmadia, A. A. A. Raman, R. Parthasarathy, and B. Sajjadi, “Sonochemical reactors: Review on features, advantages and limitations,” *Renewable and Sustainable Energy Reviews*, 2016. **63**: 302–314.
[24] B. Verhaagen and D. Fernández Rivas, “Measuring cavitation and its cleaning effect,” *Ultrasonics Sonochemistry*, 2015. **29**: 619–628.
[25] M. Hodnett, M. J. Choi, and B. Zeqiri, “Towards a reference ultrasonic cavitation vessel. Part 1: Preliminary investigation of the acoustic field distribution in a 25 kHz cylindrical cell,” *Ultrasonics Sonochemistry*, 2007. **14**(1): 29–40.
[26] M. Hodnett and B. Zeqiri, “Toward a reference ultrasonic cavitation vessel: Part 2 - Investigating the spatial variation and acoustic pressure threshold of inertial cavitation

in a 25 kHz ultrasound field," *IEEE Transactions on Ultrasonics, Ferroelectrics, and Frequency Control*, 2008. **55**(8): 1809–1822.
[27] O. Johansson, T. Lofqvist, and T. R. K. Pamidi, "Design of high-intensity ultrasound reactor," *IEEE International Ultrasonics Symposium, IUS*, 2017. .
[28] Y. A. Pishchalnikov, J. Gutierrez, W. W. Dunbar, and R. W. Philpott, "Intense cavitation at extreme static pressure," *Ultrasonics*, 2016. **65**: 380–389.
[29] Y. Asakura, K. Yasuda, D. Kato, Y. Kojima, and S. Koda, "Development of a large sonochemical reactor at a high frequency," *Chemical Engineering Journal*, 2008. **139**(2): 339–343.
[30] W. Tangsopa and J. Thongsri, "Development of an industrial ultrasonic cleaning tank based on harmonic response analysis," *Ultrasonics*, 2019. **91**(January 2018): 68–76.
[31] M. Khavari *et al.*, "Scale up design study on process vessel dimensions for ultrasonic processing of water and liquid aluminium," *Ultrasonics Sonochemistry*, 2021. **76**(May): 105647.
[32] K. Johnston *et al.*, "Periodic shock-emission from acoustically driven cavitation clouds: A source of the subharmonic signal," *Ultrasonics*, 2014. **54**(8): 2151–2158.
[33] I. Tzanakis, G. S. B. Lebon, D. G. Eskin, and K. A. Pericleous, "Characterizing the cavitation development and acoustic spectrum in various liquids," *Ultrasonics Sonochemistry*, 2017. **34**: 651–662.
[34] L. Yusuf, M. D. Symes, and P. Prentice, "Characterising the cavitation activity generated by an ultrasonic horn at varying tip-vibration amplitudes," *Ultrasonics Sonochemistry*, 2021. **70**: 105273.
[35] I. Tzanakis, M. Hodnett, G. S. B. Lebon, N. Dezhkunov, and D. G. Eskin, "Calibration and performance assessment of an innovative high-temperature cavitometer," *Sensors and Actuators, A: Physical*, 2016. **240**: 57–69.
[36] M. Khavari, A. Priyadarshi, A. Hurrell, K. Pericleous, D. Eskin, and I. Tzanakis, "Characterization of shock waves in power ultrasound," *Journal of Fluid Mechanics*, 2021. **915**.
[37] X. Song *et al.*, "Correlation between the macroscopic adhesion strength of cold spray coating and the microscopic single-particle bonding behaviour: Simulation, experiment and prediction," *Applied Surface Science*, 2021. **547**: 149165.